Received: 27 December 2020 | Revised: 15 February 2021 | Accepted: 19 February 2021

DOI: 10.1002/htj.22120

RESEARCH ARTICLE

HEAT TRANSFER WILEY

Statistical approach on 3D hydromagnetic flow of water-based nanofluid between two vertical porous plates moving in opposite directions

Thaivalappil Sugathan Neethu | **Sujesh Areekara** | **Alphonsa Mathew**

Department of Mathematics, St. Thomas' College (Autonomous), Thrissur, India

Correspondence
Alphonsa Mathew, Department of Mathematics, St. Thomas' College (Autonomous), Thrissur, Kerala 680001, India.
Email: alphonsa@stthomas.ac.in

Abstract

The nanofluid flow between two plates is a common topic of research. However, studies dealing with the flow between two vertical plates moving in different directions have not been largely accounted for. The main aim of this study is to analytically and statistically investigate the MHD flow of water-based nanofluid between two vertical porous plates moving in opposite directions using perturbation technique and multiple linear regression, respectively. The consequence of various parameters on concentration, temperature, and velocity are examined via graphs using MATLAB software. It is observed that the main flow velocity profile is greater when the magnetic field is applied on the upward moving plate as compared to the main flow velocity when the magnetic field is applied on the downward-moving plate. The physical quantities are scrutinized using statistical tools like probable error and multiple linear regression and an excellent agreement is noted. It is noted that the Nusselt number is highly positively correlated with the injection parameter and highly negatively correlated with nanoparticle volume fraction. Furthermore, the simultaneous effects of parameters

on drag coefficients are studied with the aid of three-dimensional surface plots.

KEYWORDS

correlation coefficient, natural convection, opposite moving plates, regression analysis, unsteady three-dimensional MHD flow, water-based nanofluid

1 | INTRODUCTION

Magnetohydrodynamics (MHD), the area which deals with the study of dynamics of electrically conducting fluids under the influence of magnetic field, has raised quite an interest over the years due to its versatile number of application in various fields; like in geophysics, engineering, biomedical engineering, magnetic drug targeting, and many others.

MHD is commonly paired with convective flows, which can either be natural, forced, or mixed. Natural or free convection is the type of flow where the motion is not generated by an external source. Natural convection has called in a lot of attention from the researchers with its applications ranging from engineering to nature. Sabu et al.[1] studied the behavior of hydromagnetic convective ferro-nanofluid flow through an inclined channel with porous medium and observed an increase in velocity with respect to Hall current. Kumar et al.[2] employ a numerical model to investigate the influence of thermal radiation on the nanofluid flow from an infinite vertical plate considering viscous dissipation and magnetic field. It is noted that an augmentation in radiation parameter causes an enhancement in the temperature and velocity profiles. MHD convective flow with various attributes are explained in References [3–10].

Plates containing voids (holes) are known as porous plates. The flow through porous plates has applications in chemical engineering (for filtration and clarification), agriculture (in the study of underwater resources), and petroleum industry (to study the movement of natural gas, oil, and water). Biswal et al.[11] elucidated the influence of transverse magnetic effect on the flow of water-based fluid with added silver and copper nanoparticles in a semiporous channel using the least square method. A great deal of studies has been carried out in problems dealing with the MHD flow in a porous channel as well as parallel plates.[12–21]

Nanofluids have been a hot topic for a while now. Using nanofluids instead of the normal base fluids has yielded many awarding results. It is seen that nanofluids have better convective heat transfer capabilities. Kiyani et al.[22] semianalytically investigated the bidirectional Williamson nanofluid flow in porous space using optimal homotopy asymptotic method (OHAM) and observed that space- and temperature-dependent heat sources have a positive effect on temperature. Kumar et al.[23] studied magnetite water-based nanofluid flow over a rotating disk in the presence of an external magnetic field and Arrhenius activation energy using fourth-order Noumerov's method and noted that the thermophoresis parameter has a negative impact on heat transfer rate. Hazarika et al.[24] used the fourth-order Runge-Kutta-shooting technique to numerically investigate the MHD flow of a chemically reacting water-based nanofluid over a permeable stretching sheet involving chemical reaction, thermophoresis, heat source, and viscous dissipation. Seth et al.[25] examined the unsteady hydromagnetic boundary layer flow of a thermally radiating nanofluid considering Navier's velocity slip and external magnetic field past nonlinear stretching sheet placed in a porous medium using

OHAM. Furthermore, linear and quadratic multiple linear regression analysis was exercised in scrutinizing the effect of pertinent parameters on Nusselt number and drag coefficient.

The use of statistical tools for analyzing the effects of numerous physical parameters has intrigued a lot of researchers. A countable number of works, where the ideas of correlation, slope of linear regression, probable error, and regression analysis are used to compare and analyze the outcome of various physical quantities,[1,26–32] have been published.

Many researchers have analyzed the hydromagnetic flow between two vertical porous plates due to free convection and varying geometrical shapes. However, only a countable number of works involving MHD-free convective flow between two vertical porous plates moving in differing direction[33–36] have been published. Previous studies were based on conventional (base) fluids, whereas the present study extends the problem into nanoscale. The current problem finds its application in several engineering, geophysical, and industrial fields. The problem is solved using the perturbation technique. Results are presented with the help of tables and graphs. Mass and heat transfer rates are analyzed and modeled using statistical tools like probable error and regression.

2 | PROBLEM STATEMENT

An unsteady hydromagnetic fluctuating flow of a water-based nanofluid between two insulated vertical porous plates is considered (Figure 1). The problem is studied under the following assumptions:

(i) Plates are moving in opposite directions with uniform velocity.
(ii) The upward moving plate is subjected to a transverse sinusoidal injection velocity, whereas the downward-moving plate is subjected to a constant suction velocity.
(iii) A magnetic field of uniform strength is applied perpendicular to the plane of the plate.
(iv) The induced magnetic field has been neglected due to the assumption of a small magnetic Reynolds number.
(v) The nanofluid constants are taken in accordance with Table 1.
(vi) The injection velocity distribution is of the form

TABLE 1 Nanofluid constants

Effective dynamic viscosity	$\frac{1}{A_1} = \frac{\mu_{nf}}{\mu_f} = \frac{1}{(1-\phi)^{2.5}}$
Effective density	$A_2 = \frac{\rho_{nf}}{\rho_f} = (1-\phi) + \phi\left(\frac{\rho_s}{\rho_f}\right)$
Effective electrical conductivity	$A_3 = \frac{\sigma_{nf}}{\sigma_f} = 1 + \frac{3\left(\frac{\sigma_s}{\sigma_f} - 1\right)\phi}{\left(\frac{\sigma_s}{\sigma_f} + 2\right) - \left(\frac{\sigma_s}{\sigma_f} - 1\right)\phi}$
Effective coefficient of thermal expansion	$A_4 = \frac{\beta_{nf}}{\beta_f} = (1-\phi) + \phi\left(\frac{\beta_s}{\beta_f}\right)$
Effective specific heat	$A_5 = \frac{(\rho C_p)_{nf}}{(\rho C_p)_f} = (1-\phi) + \phi\left(\frac{(\rho C_p)_s}{(\rho C_p)_f}\right)$
Effective thermal conductivity	$A_6 = \frac{\kappa_{nf}}{\kappa_f} = \frac{\kappa_s + 2\kappa_f - 2\phi(\kappa_f - \kappa_s)}{\kappa_s + 2\kappa_f + 2\phi(\kappa_f - \kappa_s)}$

$$v^*(z^*) = V_0(1 + \varepsilon_1 \cos(\pi z^*/d)).$$

(vii) Without loss of generality, the distance d between the plates is taken equal to the wavelength of the injection velocity.

(viii) The temperature of the upward moving plate fluctuating with time is given as

$$T^*(t^*) = T_0 + \varepsilon_2(T_0 - T_1)e^{i\omega^* t^*}.$$

(ix) The concentration of the upward moving plate fluctuating with time is given as

$$C^*(t^*) = \mathcal{C}_0 + \varepsilon_3(\mathcal{C}_0 - \mathcal{C}_1)e^{i\omega^* t^*}.$$

(x) The temperature and concentration of the downward-moving plate are at constant temperature T_1 and constant concentration $\mathcal{C}_1$, respectively.

Using the above assumptions and Boussinesq's approximation, the governing equations[33] takes the form:

$$\frac{\partial v^*}{\partial y^*} + \frac{\partial w^*}{\partial z^*} = 0, \tag{1}$$

$$\frac{\partial u^*}{\partial t^*} + v^*\frac{\partial u^*}{\partial y^*} + w^*\frac{\partial u^*}{\partial z^*} = -\frac{1}{\rho_{\mathrm{nf}}}\left[\frac{\partial p^*}{\partial x^*} - \mu_{\mathrm{nf}}\left(\frac{\partial^2 u^*}{\partial y^{*2}} + \frac{\partial^2 u^*}{\partial z^{*2}}\right) + \sigma_{\mathrm{nf}} B_0^2 u^*\right] + g\beta_{\mathrm{nf}}(T^* - T_1) + g\beta_{\mathrm{nf}}(C^* - \mathcal{C}_1), \tag{2}$$

$$\frac{\partial v^*}{\partial t^*} + v^*\frac{\partial v^*}{\partial y^*} + w^*\frac{\partial v^*}{\partial z^*} = -\frac{1}{\rho_{\mathrm{nf}}}\left[\frac{\partial p^*}{\partial y^*} - \mu_{\mathrm{nf}}\left(\frac{\partial^2 v^*}{\partial y^{*2}} + \frac{\partial^2 v^*}{\partial z^{*2}}\right)\right], \tag{3}$$

$$\frac{\partial w^*}{\partial t^*} + v^*\frac{\partial w^*}{\partial y^*} + w^*\frac{\partial w^*}{\partial z^*} = -\frac{1}{\rho_{\mathrm{nf}}}\left[\frac{\partial p^*}{\partial z^*} - \mu_{\mathrm{nf}}\left(\frac{\partial^2 w^*}{\partial y^{*2}} + \frac{\partial^2 w^*}{\partial z^{*2}}\right) + \sigma_{\mathrm{nf}} B_0^2 w^*\right], \tag{4}$$

$$\frac{\partial T^*}{\partial t^*} + v^*\frac{\partial T^*}{\partial y^*} + w^*\frac{\partial T^*}{\partial z^*} = \frac{\kappa_{\mathrm{nf}}}{(\rho c_p)_{\mathrm{nf}}}\left[\frac{\partial^2 T^*}{\partial y^{*2}} + \frac{\partial^2 T^*}{\partial z^{*2}}\right], \tag{5}$$

$$\frac{\partial C^*}{\partial t^*} + v^*\frac{\partial C^*}{\partial y^*} + w^*\frac{\partial C^*}{\partial z^*} = D_B\left(\frac{\partial^2 C^*}{\partial y^{*2}} + \frac{\partial^2 C^*}{\partial z^{*2}}\right) - K_l(C^* - \mathcal{C}_1). \tag{6}$$

The boundary conditions for the problem are:

$$\left.\begin{array}{c} y^* = 0,\ u^* = U_0,\ v^*(z^*) = V_0\left(1 + \varepsilon_1 \cos\dfrac{\pi z^*}{d}\right),\ w^* = 0, \\ T^*(t^*) = T_0 + \varepsilon_2(T_0 - T_1)e^{i\omega^* t^*},\ C^*(t^*) = \mathcal{C}_0 + \varepsilon_3(\mathcal{C}_0 - \mathcal{C}_1)e^{i\omega^* t^*} \\ y^* = d,\ u^* = -U_0,\ v^*(z^*) = V_0,\ w^* = 0,\ T^* = T_1,\ C^* = \mathcal{C}_1 \end{array}\right\} \tag{7}$$

Introducing the following nondimensional quantities

$$y = \frac{y^*}{d}, z = \frac{z^*}{d}, t = t^*\omega^*, u = \frac{u^*}{U_0}, v = \frac{v^*}{V_0}, w = \frac{w^*}{V_0},$$
$$\omega = \frac{\omega^* d^2}{\vartheta}, p = \frac{p^*}{\rho_{nf} V_0^2}, \theta = \frac{T^* - T_1}{T_0 - T_1}, C = \frac{C^* - C_1}{C_0 - C_1}$$

into Equations (1)–(7), excluding (2) we get:

$$\frac{\partial v}{\partial y} + \frac{\partial w}{\partial z} = 0, \tag{8}$$

$$\frac{\omega}{Re}\frac{\partial v}{\partial t} + v\frac{\partial v}{\partial y} + w\frac{\partial v}{\partial z} = -\frac{\partial p}{\partial y} + \frac{1}{A_1 A_2 Re}\left(\frac{\partial^2 v}{\partial y^2} + \frac{\partial^2 v}{\partial z^2}\right), \tag{9}$$

$$\frac{\omega}{Re}\frac{\partial w}{\partial t} + v\frac{\partial w}{\partial y} + w\frac{\partial w}{\partial z} = -\frac{\partial p}{\partial z} + \frac{1}{A_1 A_2 Re}\left(\frac{\partial^2 w}{\partial y^2} + \frac{\partial^2 w}{\partial z^2}\right) - \frac{A_3}{A_2 Re}H^2 w, \tag{10}$$

$$\frac{\omega}{Re}\frac{\partial \theta}{\partial t} + v\frac{\partial \theta}{\partial y} + w\frac{\partial \theta}{\partial z} = \frac{A_6}{A_5 PrRe}\left(\frac{\partial^2 \theta}{\partial y^2} + \frac{\partial^2 \theta}{\partial z^2}\right), \tag{11}$$

$$\frac{\omega}{Re}\frac{\partial C}{\partial t} + v\frac{\partial C}{\partial y} + w\frac{\partial C}{\partial z} = \frac{1}{ReSc}\left(\frac{\partial^2 C}{\partial y^2} + \frac{\partial^2 C}{\partial z^2}\right) - \frac{Kr}{Re}C. \tag{12}$$

Equation (2) reduces to the following partial differential equations based on the two cases:
Case 1: Magnetic field is applied on the upward moving plate (at $y = 0$)

$$\frac{\omega}{Re}\frac{\partial u}{\partial t} + v\frac{\partial u}{\partial y} + w\frac{\partial u}{\partial z} = \frac{1}{A_1 A_2 Re}\left(\frac{\partial^2 u}{\partial y^2} + \frac{\partial^2 u}{\partial z^2}\right) - \frac{A_3}{A_2 Re}H^2(u - 1) + A_4 GrRe\theta + A_4 GmReC. \tag{13}$$

Case 2: Magnetic field is applied on the downward-moving plate (at $y = 1$)

$$\frac{\omega}{Re}\frac{\partial u}{\partial t} + v\frac{\partial u}{\partial y} + w\frac{\partial u}{\partial z} = \frac{1}{A_1 A_2 Re}\left(\frac{\partial^2 u}{\partial y^2} + \frac{\partial^2 u}{\partial z^2}\right) - \frac{A_3}{A_2 Re}H^2(u + 1) + A_4 GrRe\theta + A_4 GmReC, \tag{14}$$

where the nondimensional parameters are explained in the nomenclature.

The boundary conditions in the nondimensional form are given by

$$\left.\begin{array}{llllll} y = 0, & u = 1, & v(z) = 1 + \varepsilon_1 \cos \pi z, & w = 0, & \theta = 1 + \varepsilon_2 e^{it}, & C = 1 + \varepsilon_3 e^{it} \\ y = 1, & u = -1, & v = 1, & w = 0, & \theta = 0, & C = 0 \end{array}\right\} \tag{15}$$

3 | METHODOLOGY

Since $\varepsilon = \min\{\varepsilon_1, \varepsilon_2, \varepsilon_3\}$ is very small, we assume that the solution of the problem is of the form

$$f(y, z, t) = f_0(y) + \varepsilon f_1(y, z, t) + O(\varepsilon^2). \tag{16}$$

3.1 | Steady flow solution

When $\varepsilon = 0$, the current problem contracts to a steady two-dimensional hydromagnetic flow between two vertical porous plates moving in different directions with uniform injection/suction, which is governed by the following equations:

Case 1: Magnetic field is applied on the upward moving plate (at $y = 0$)

$$u_0'' - A_1A_2Reu_0' - A_1A_3H^2(u_0 - 1) + A_1A_2A_4Re^2\,Gr\theta_0 + A_1A_2A_4Re^2\,GmC_0 = 0. \tag{17}$$

Case 2: Magnetic field is applied on the downward moving plate (at $y = 1$)

$$u_0'' - A_1A_2Reu_0' - A_1A_3H^2(u_0 + 1) + A_1A_2A_4Re^2\,Gr\theta_0 + A_1A_2A_4Re^2\,GmC_0 = 0, \tag{18}$$

with $v_0 = 1, w_0 = 0, p_0 = \text{constant}$ and

$$\theta_0'' - \frac{A_5PrRe}{A_6}\theta_0' = 0, \tag{19}$$

$$C_0'' - ScReC_0' - KrScC_0 = 0, \tag{20}$$

where primes denote the derivative with respect to y.

The corresponding boundary condition for the above two cases reduce to:

$$\left.\begin{array}{c} y = 0, u_0 = 1, \theta_0 = 1, C_0 = 1 \\ y = 1, u_0 = -1, \theta_0 = 0, C_0 = 0 \end{array}\right\} \tag{21}$$

The solutions of Equations (17)–(20) subject to (21) are:

$$\theta_0 = \frac{1}{e^a - 1}(e^a - e^{ay}), \tag{22}$$

$$C_0 = \frac{1}{(e^{m_2} - e^{m_1})}(e^{m_2}e^{m_1y} - e^{m_1}e^{m_2y}). \tag{23}$$

Case 1: Magnetic field is applied on the upward moving plate (at $y = 0$)

$$u_0 = \frac{1}{(e^{m_4} - e^{m_3})}((\alpha_1e^{m_4} - \beta_1)e^{m_3y} + (\beta_1 - \alpha_1e^{m_3})e^{m_4y}) + B_1e^{ay} + B_2e^{m_1y} + B_3e^{m_2y} + B_4 + 1 \tag{24}$$

Case 2: Magnetic field is applied on the downward moving plate (at $y = 1$)

$$u_0 = \frac{1}{(e^{m_4} - e^{m_3})}(((\alpha_1 + 2)e^{m_4} - (\beta_1 + 2))e^{m_3y} + ((\beta_1 + 2) - (\alpha_1 + 2)e^{m_3})e^{m_4y}) + B_1e^{ay} + B_2e^{m_1y} + B_3e^{m_2y} + B_4 - 1. \tag{25}$$

3.2 | Cross flow solution

When $\varepsilon \neq 0$, substituting Equation (16) in Equations (8)–(10) and comparing the coefficients of ε and neglecting the terms with $O(\varepsilon^2)$, we obtain the following first-order equations:

$$\frac{\partial v_1}{\partial y} + \frac{\partial w_1}{\partial z} = 0, \tag{26}$$

$$\frac{\omega}{Re}\frac{\partial v_1}{\partial t} + \frac{\partial v_1}{\partial y} = -\frac{\partial p_1}{\partial y} + \frac{1}{A_1 A_2 Re}\left(\frac{\partial^2 v_1}{\partial y^2} + \frac{\partial^2 v_1}{\partial z^2}\right), \tag{27}$$

$$\frac{\omega}{Re}\frac{\partial w_1}{\partial t} + \frac{\partial w_1}{\partial y} = -\frac{\partial p_1}{\partial z} + \frac{1}{A_1 A_2 Re}\left(\frac{\partial^2 w_1}{\partial y^2} + \frac{\partial^2 w_1}{\partial z^2}\right) - \frac{A_3}{A_2 Re}H^2 w_1. \tag{28}$$

Corresponding boundary conditions are

$$\left.\begin{array}{c} y = 0, v_1 = \cos \pi z, w_1 = 0 \\ y = 1, v_1 = 0, w_1 = 0 \end{array}\right\}. \tag{29}$$

These are the linear partial differential equations describing the three-dimensional cross-flow, which is independent of the main flow component, u_1, temperature field, θ_1, and concentration field, C_1.

Assume that the solutions for v_1, w_1, p_1 are of the form:

$$v_1(y, z, t) = v_{11}(y)e^{it} + v_{12}(y)\cos \pi z, \tag{30}$$

$$w_1(y, z, t) = -\left(z v'_{11}(y)e^{it} + \frac{1}{\pi}v'_{12}(y)\sin \pi z\right), \tag{31}$$

$$p_1(y, z, t) = p_{11}(y)e^{it} + p_{12}(y)\cos \pi z, \tag{32}$$

where prime denotes the derivative with respect to y. Expressions (30) and (31) are chosen in such a way that the continuity Equation (26) is precisely satisfied. Substituting these into Equations (27) and (28) and applying Equation (29), we obtain the solutions of v_1, w_1, p_1 as:

$$v_1 = \frac{1}{D}\sum_{i=1}^{4} D_i e^{r_i y}\cos \pi z, \tag{33}$$

$$w_1 = -\frac{1}{\pi D}\sum_{i=1}^{4} r_i D_i e^{r_i y}\sin \pi z, \tag{34}$$

$$p_1 = \frac{1}{A_1 A_2 Re \pi^2 D}\sum_{i=1}^{4} D_i (r_i^3 - A_1 A_2 Re r_i^2 - (A_1 A_3 H^2 + \pi^2) r_i) e^{r_i y}\cos \pi z. \tag{35}$$

3.3 | Temperature and concentration field

Similarly, using Equation (16) when $\varepsilon \neq 0$, the first-order equation for temperature and concentration fields are

$$\frac{\omega}{Re}\frac{\partial\theta_1}{\partial t}+\frac{\partial\theta_1}{\partial y}=\frac{A_6}{A_5 PrRe}\left(\frac{\partial^2\theta_1}{\partial y^2}+\frac{\partial^2\theta_1}{\partial z^2}\right), \tag{36}$$

$$\frac{\omega}{Re}\frac{\partial C_1}{\partial t}+\frac{\partial C_1}{\partial y}=\frac{1}{ReSc}\left(\frac{\partial^2 C_1}{\partial y^2}+\frac{\partial^2 C_1}{\partial z^2}\right)-\frac{Kr}{Re}C_1, \tag{37}$$

with corresponding boundary conditions

$$\left.\begin{array}{l} y=0,\theta_1=e^{it},C_1=e^{it} \\ y=1,\theta_1=0,C_1=0 \end{array}\right\}. \tag{38}$$

Equations (36)–(38) are solved with an assumption that the solutions are of the form:

$$\theta_1(y,z,t)=\theta_{11}e^{it}+\theta_{12}\cos\pi z, \tag{39}$$

$$C_1(y,z,t)=C_{11}e^{it}+C_{12}\cos\pi z. \tag{40}$$

Substituting Equations (39) and (40) in (36) and (37), respectively we get

$$\theta_{11}''-\frac{A_5 PrRe}{A_6}\theta_{11}'-\frac{A_5 Pr\omega i}{A_6}\theta_{11}=0, \tag{41}$$

$$\theta_{12}''-\frac{A_5 PrRe}{A_6}\theta_{12}'-\pi^2\theta_{12}=0, \tag{42}$$

$$C_{11}''-ScReC_{11}'-(Sc\omega i+KrSc)C_{11}=0, \tag{43}$$

$$C_{12}''-ScReC_{12}'-(ScKr+\pi^2)C_{12}=0, \tag{44}$$

with the corresponding transformed boundary conditions

$$\left.\begin{array}{l} y=0,\theta_{11}=1,\theta_{12}=0,C_{11}=1,C_{12}=0 \\ y=1,\theta_{11}=0,\theta_{12}=0,C_{11}=0,C_{12}=0 \end{array}\right\}. \tag{45}$$

Solving Equations (41)–(44) under the boundary condition (45), the solutions are obtained as

$$\theta_1(y,z,t)=\frac{1}{e^{n_2}-e^{n_1}}(e^{n_2}e^{n_1 y}-e^{n_1}e^{n_2 y})e^{it}, \tag{46}$$

$$C_1(y,z,t)=\frac{1}{e^{m_6}-e^{m_5}}(e^{m_6}e^{m_5 y}-e^{m_5}e^{m_6 y})e^{it}. \tag{47}$$

3.4 | Main flow solution

When $\varepsilon\neq 0$, with the aid of Equation (16) and comparing coefficients of ε, we deduce the first-order equation for the main flow component, u_1 as:

$$\frac{\omega}{Re}\frac{\partial u_1}{\partial t}+\frac{\partial u_1}{\partial y}+v_1 u_0{}'=\frac{1}{A_1A_2Re}\left(\frac{\partial^2 u_1}{\partial y^2}+\frac{\partial^2 u_1}{\partial z^2}\right)-\frac{A_3}{A_2Re}H^2u_1+A_4GrRe\theta_1+A_4GmReC_1. \tag{48}$$

The corresponding boundary conditions are:

$$\left.\begin{array}{l} y = 0, u_1 = 0 \\ y = 1, u_1 = 0 \end{array}\right\}. \tag{49}$$

To solve the above differential equation for the main flow velocity component, $u_1(y, z, t)$, we assume that the solution is of the form:

$$u_1(y, z, t) = u_{11}e^{it} + u_{12}\cos\pi z. \tag{50}$$

Substituting Equation (50) in (48) and neglecting terms of $O(\varepsilon^2)$ we obtain:

$$u_{11}'' - A_1A_2Reu_{11}' - (A_1A_2\omega i + A_1A_3H^2)u_{11} = -A_1A_2A_4Re^2\,Gr\theta_{11} - A_1A_2A_4Re^2\,GmC_{11}, \tag{51}$$

$$u_{12}'' - A_1A_2Reu_{12}' - (\pi^2 + A_1A_3H^2)u_{12} = A_1A_2Rev_{12}u_0', \tag{52}$$

with

$$\left.\begin{array}{l} y = 0, u_{11} = 0, u_{12} = 0 \\ y = 1, u_{11} = 0, u_{12} = 0 \end{array}\right\}. \tag{53}$$

Solving Equations (51) and (52) considering (53) and using (50), we derive the solutions as:
Case 1: Magnetic Field is applied on the upward moving plate (at $y = 0$)

$$\begin{aligned} u_1(y, z, t) &= \left\{\begin{array}{c} \frac{1}{e^{r_6} - e^{r_5}}[(\alpha_2e^{r_6} - \beta_2)e^{r_5y} + (\beta_2 - \alpha_2e^{r_5})e^{r_6y}] + K_1e^{n_1y} \\ + K_2\,e^{n_2y} + K_3e^{m_5y} + K_4e^{m_6y} \end{array}\right\}e^{it} \\ &+ \left\{\begin{array}{c} \frac{1}{e^{n_4} - e^{n_3}}[(\alpha_3e^{n_4} - \beta_3)e^{n_3y} + (\beta_3 - \alpha_3e^{n_3})e^{n_4y}] \\ +\sum_{i=1}^{4}(K_{i1}e^{(r_i+m_3)y} + K_{i2}e^{(r_i+m_4)y} + K_{i3}e^{(r_i+a)y} + K_{i4}e^{(r_i+m_1)y} + K_{i5}e^{(r_i+m_2)y}) \end{array}\right\}\cos\pi z \end{aligned} \tag{54}$$

Case 2: Magnetic Field is applied on the downward moving plate (at $y = 1$)

$$\begin{aligned} u_1(y, z, t) &= \left\{\begin{array}{c} \frac{1}{e^{r_6} - e^{r_5}}[(\alpha_2e^{r_6} - \beta_2)e^{r_5y} + (\beta_2 - \alpha_2e^{r_5})e^{r_6y}] + K_1e^{n_1y} \\ + K_2\,e^{n_2y} + K_3e^{m_5y} + K_4e^{m_6y} \end{array}\right\}e^{it} \\ &+ \left\{\begin{array}{c} \frac{1}{e^{n_4} - e^{n_3}}[(\alpha_4e^{n_4} - \beta_4)e^{n_3y} + (\beta_4 - \alpha_4e^{n_3})e^{n_4y}] \\ +\sum_{i=1}^{4}(M_{i1}e^{(r_i+m_3)y} + M_{i2}e^{(r_i+m_4)y} + M_{i3}e^{(r_i+a)y} + M_{i4}e^{(r_i+m_1)y} + M_{i5}e^{(r_i+m_2)y}) \end{array}\right\}\cos\pi z \end{aligned} \tag{55}$$

4 | DRAG COEFFICIENT AND TRANSFER RATES

For practical analysis of the problem, scientists, and engineers are always interested in understanding the physical quantities like Sherwood number, Nusselt number, and skin-friction coefficients as they measure the rate of mass and heat transfer and surface drag, respectively. Their modified form[33] are given by:

$$Sh = \frac{d}{D_B\left(\mathcal{C}_0 - \mathcal{C}_1\right)}\left|D_B\left(\frac{dC^*}{dy^*}\right)_{y^*=d}\right| = \left|\left(\frac{dC_0}{dy}\right)_{y=1} + \varepsilon\left(\frac{dC_1}{dy}\right)_{y=1}\right|, \tag{56}$$

$$Nu = \frac{d}{\kappa_f\left(T_0 - T_1\right)}\left|\kappa_{nf}\left(\frac{dT^*}{dy^*}\right)_{y^*=d}\right| = A_6\left|\left(\frac{d\theta_0}{dy}\right)_{y=1} + \varepsilon\left(\frac{d\theta_1}{dy}\right)_{y=1}\right|. \tag{57}$$

Case 1: Magnetic field is applied on the upward moving plate (at $y = 0$)

$$Cf = \frac{d}{\mu_f U_0}\left|\mu_{\mathrm{nf}}\left(\frac{du^*}{dy^*}\right)_{y^*=d}\right| = \frac{1}{A_1}\left|\left(\frac{du_0}{dy}\right)_{y=1} + \varepsilon\left(\frac{du_1}{dy}\right)_{y=1}\right|. \tag{58}$$

Case 2: Magnetic field is applied on the downward moving plate (at $y = 1$)

$$Cf = \frac{d}{\mu_{\mathrm{f}} U_0}\left|\mu_{\mathrm{nf}}\left(\frac{du^*}{dy^*}\right)_{y^*=d}\right| = \frac{1}{A_1}\left|\left(\frac{du_0}{dy}\right)_{y=1} + \varepsilon\left(\frac{du_1}{dy}\right)_{y=1}\right|. \tag{59}$$

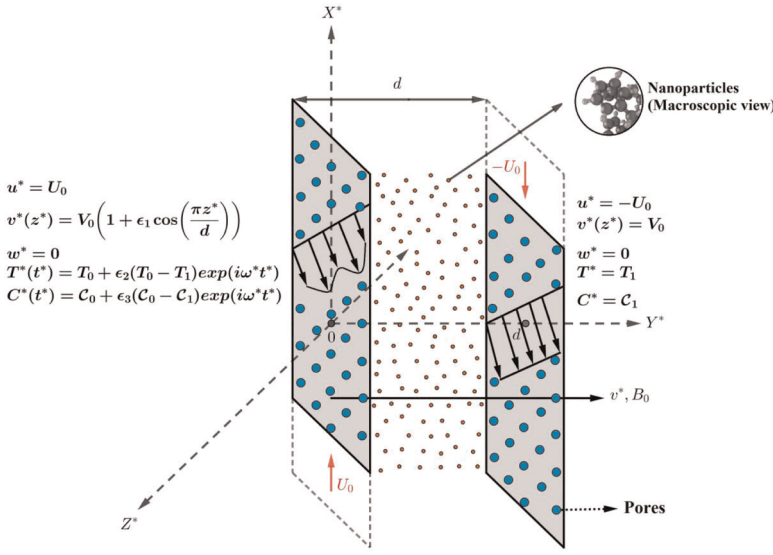

FIGURE 1 Figurative representation [Color figure can be viewed at wileyonlinelibrary.com]

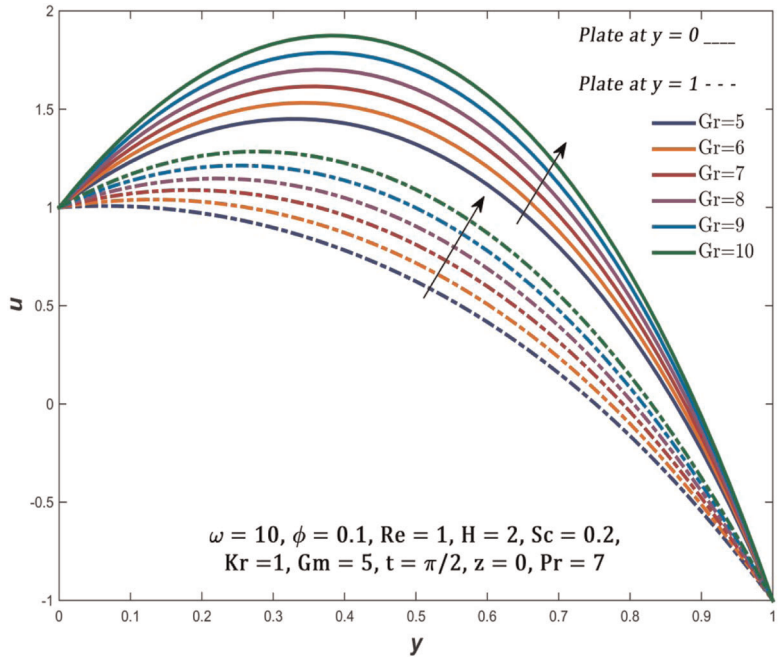

FIGURE 2 Change in u with Gr [Color figure can be viewed at wileyonlinelibrary.com]

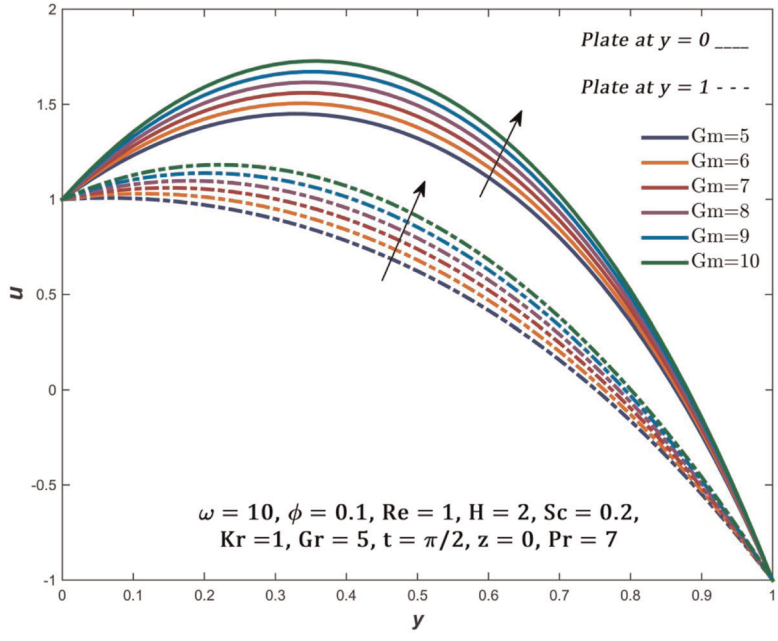

FIGURE 3 Change in u with Gm [Color figure can be viewed at wileyonlinelibrary.com]

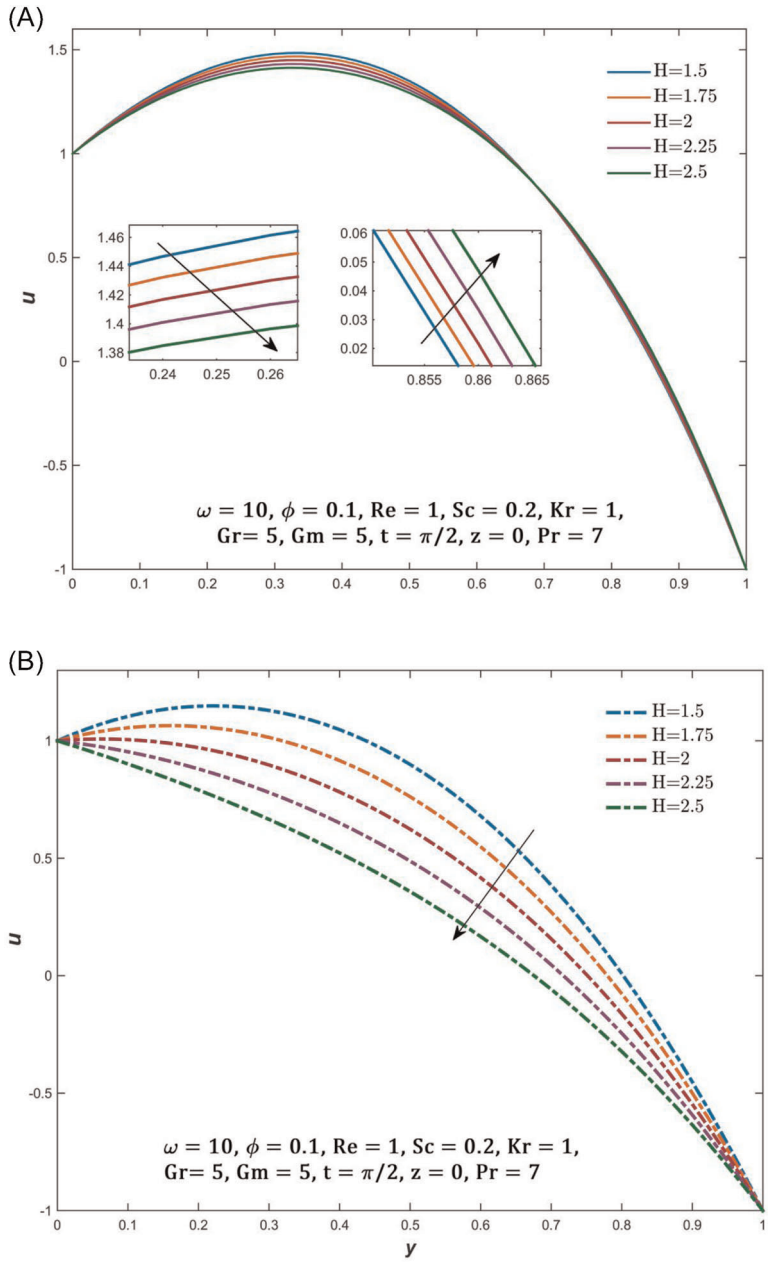

FIGURE 4 (A) Change in u with H for plate at $y = 0$. (B) Change in u with H for plate at $y = 1$ [Color figure can be viewed at wileyonlinelibrary.com]

5 | RESULTS AND DISCUSSIONS

The impact of various nanofluids, the volume fraction of nanoparticle (ϕ), Grashof number (Gr), chemical reaction parameter (Kr), injection/suction parameter (Re), Schmidt number (Sc), Hartmann number (H), and modified Grashof number (Gm) on concentration (C), temperature

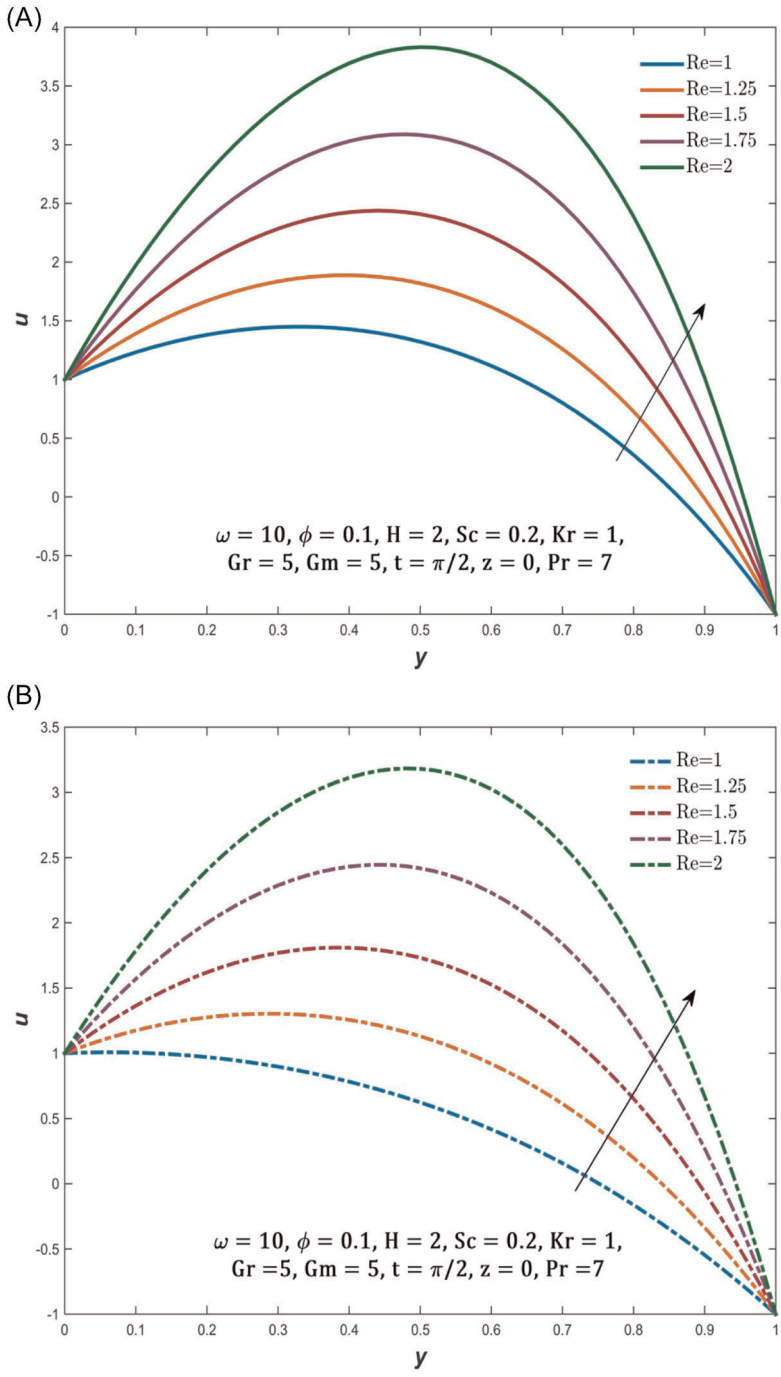

FIGURE 5 (A) Change in u with Re for plate at $y = 0$. (B) Change in u with Re for plate at $y = 1$ [Color figure can be viewed at wileyonlinelibrary.com]

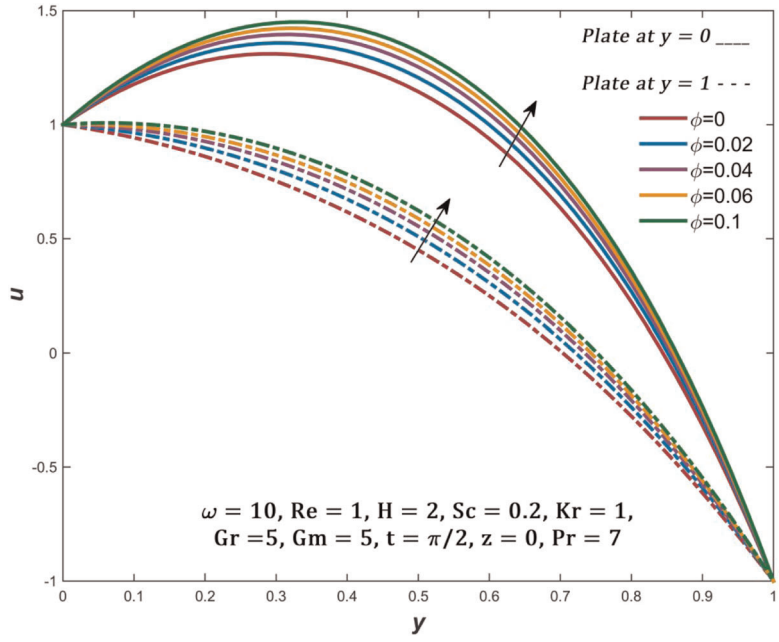

FIGURE 6 Change in u with ϕ [Color figure can be viewed at wileyonlinelibrary.com]

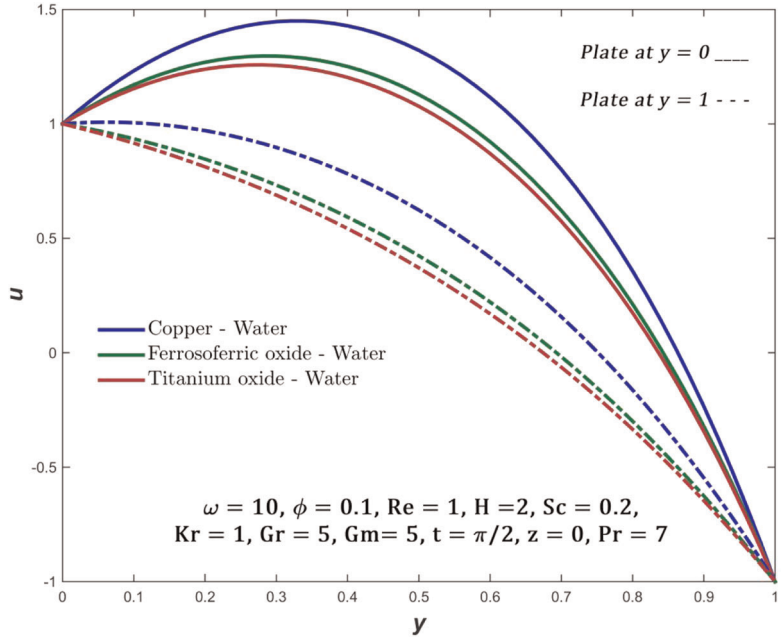

FIGURE 7 Change in u with different nanofluids [Color figure can be viewed at wileyonlinelibrary.com]

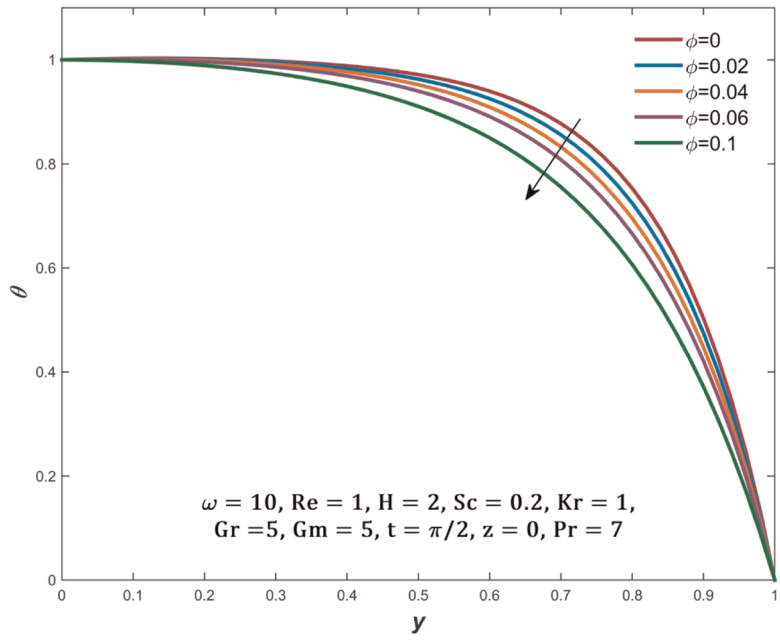

FIGURE 8 Change in θ with ϕ [Color figure can be viewed at wileyonlinelibrary.com]

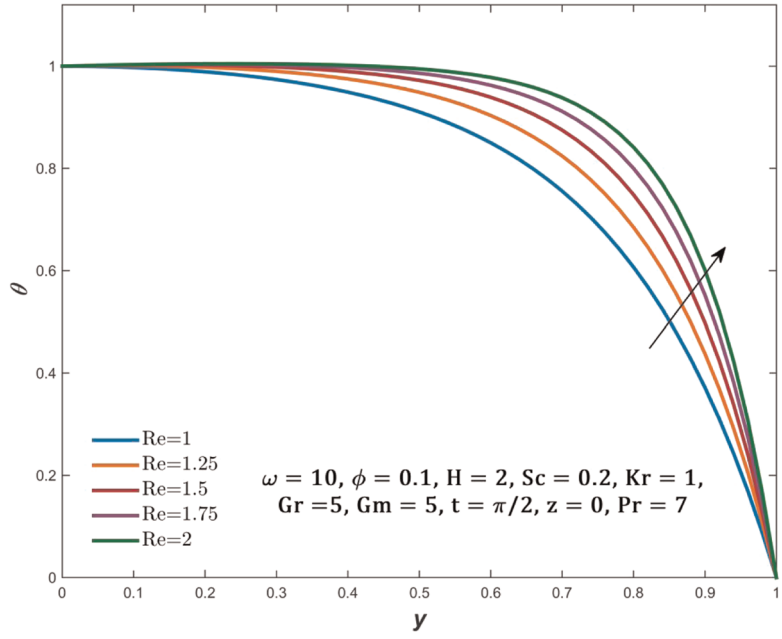

FIGURE 9 Change in θ with *Re* [Color figure can be viewed at wileyonlinelibrary.com]

(θ), and velocity (u) profiles are analyzed in Figures 2–10. The analysis has been carried out for Cu–H_2O nanofluid at $z = 0, t = \pi/2$ and $Pr = 7$. The thermophysical properties of the base fluid and nanoparticles are given in Table 2.

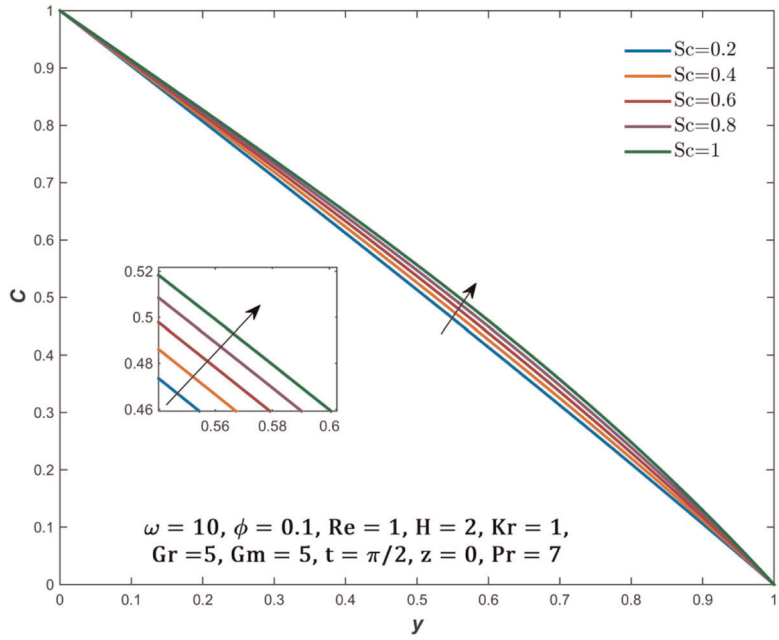

FIGURE 10 Change in C with Sc [Color figure can be viewed at wileyonlinelibrary.com]

TABLE 2 Thermophysical properties of base fluid and nanoparticles

Physical properties	H_2O[1]	Cu[30]	TiO_2[30]	Fe_3O_4[1]
ρ	997.1	8933	4250	5180
C_p	4179	385	686.2	670
β	21×10^5	1.67×10^5	0.9×10^5	1.3×10^5
σ	5×10^{-2}	5.96×10^7	2.38×10^6	25000
κ	0.613	400	8.9538	9.7

The consequence of Gr, the ratio of buoyancy force to viscous force, on u is presented in Figure 2. An increase in Gr causes augmentation in u for both cases (magnetic field fixed with the upward and downward moving plate). Physically, an increase in Gr paves to the increase in buoyancy force, which, in turn, increases the velocity. Figure 3 confirms that u increases in both cases when Gm is increased, the physical reason being the increase in buoyancy force due to a concentration difference. The influence of H, ratio of electromagnetic force to the viscous force, on u is graphed in Figure 4A,B. It is evident that a rise in H drastically reduces the velocity in the case of a downward moving plate. Physically, this is due to the fact that the presence of a magnetic field induces a Lorentz force against the fluid flow, which retards the velocity profile. However, in the case of an upward-moving plate, H expresses a mixed behavior on u. In the beginning, an increase in H reduces the velocity, but after a certain distance, the behavior is reversed. Figure 5A,B illustrates the exponential increase in $u\{\text{both cases}\}$ corresponding to the augmentation in Re. Figure 6 depicts the positive impact of ϕ on u. The impact of various nanofluids (water-based $Cu/Fe_3O_4/TiO_2$ nanofluid) on u is depicted in Figure 7.

TABLE 3 Variation in Nu for differing parameter values at $y = 1$ when $\phi = 0.02$, $\omega = 5$, $Re = 1$, $t = \pi/2$, $z = 0$ and $Pr = 7$

t	ϕ	ω	Re	Nu	Enhancement/ decrement rate (%)
0.5				6.967725	
1				6.980359	0.18
1.5				6.994532	0.20
Slope				**0.026808**	
	0.01			7.004436	
	0.02			6.996461	−0.11
	0.03			6.989177	−0.10
Slope				**−0.762966**	
		5		6.996461	
		6		6.985502	−0.16
		7		6.979319	−0.09
Slope				**−0.008571**	
			1	6.996461	
			1.1	7.693704	9.97
			1.2	8.393986	9.10
Slope				**6.987624**	

The effect of ϕ on θ is elucidated in Figure 8. ϕ has a negative impact on the temperature profile, meaning an increase in ϕ fuels a decrease in θ. Figure 9 depicts the consequence of Re on temperature. It is observed that Re induces an increase in θ. The influence of Sc on C is illustrated in Figure 10. Concentration profile (C) experiences a slight increase when Sc values are improved.

The consequence of heat and mass transfer rate on fluctuating parameters along with the slope of linear regression via data points and the enhancement/decrement rate is assessed in Tables 3 and 4, respectively. A negative sign in slope and enhancement/decrement rate symbolizes that the corresponding parameter has a negative impact on heat and mass transfer, meaning augmentation in parameter reduces the heat and mass transfer rate, while the magnitude of slope represents the quantity of change.

It is observed that t and Re have a positive impact on Nu and ϕ, and ω have a negative impact on Nu. The respective rates (slope) are shown in Table 3. For Sh, when all other parameters are kept constant, Sh increases with an increase in ω at the rate of 0.000322, Re at 0.104051, and Sc at 0.355898. Also, when Kr and t increases Sh decreases at the rate of 0.03518 and 0.00751, respectively. Figures 11 and 12 describe the parallel effect of $\phi - Re$ and $H - Gr$ on Cf. From 11a and 12a, it can be deduced that ϕ, Re, H, and Gr promotes Cf on the upward moving plate. From 11b and 12b, it can be summarized that ϕ, Re,andGr promotes Cf, while H demotes Cf on the downward-moving plate.

TABLE 4 Variation in Sh for differing parameter values at $y = 1$ when $\omega = 5$, $Re = 1$, $Sc = 0.2$, $Kr = 1$, $t = \pi/2$, $z = 0$ and $Pr = 7$

t	ω	Re	Sc	Kr	Sh	Enhancement/ decrement rate
0.5					1.077447	
1					1.074565	−0.27
1.5					1.069938	−0.43
Slope					**−0.00751**	
	5				1.069202	
	6				1.069538	0.03
	7				1.069867	0.03
Slope					**0.000332**	
		1			1.069202	
		1.1			1.079575	0.97
		1.2			1.090013	0.97
Slope					**0.104051**	
			0.2		1.069202	
			0.4		1.139795	6.60
			0.6		1.211562	6.30
Slope					**0.355898**	
				0.5	1.086993	
				1	1.069202	−1.64
				1.5	1.051816	−1.63
Slope					**−0.03518**	

6 | STATISTICAL ANALYSIS

6.1 | Correlation and probable error

Correlation, a statistical technique, which enables the user to find the degree of relationship between two or more variables, has gained a lot of interest in recent times. The effects of different parameters on Nu and Sh are comprehensively carried out and established using tables. A more detailed study is carried out with the help of correlation coefficient (r) and probable error (PE). The nature and the intensity of the relationship are communicated through the sign and magnitude of r, respectively. PE of r helps in determining the accuracy and reliability of the calculated correlation coefficient. According to Fisher,[37] correlation is said to be significant if $|\frac{r}{PE}| > 6$, where probable error, $PE = (\frac{1-r^2}{\sqrt{n}})0.6745$ and n is the number of observations.

From Table 5, we can infer that Nu is highly negatively correlated with ϕ and ω and highly positively correlated with Re and t. From $|\frac{r}{PE}|$ values, we can conclude that all parameters are significant. Table 6 proposes that Sh is highly positively correlated with ω, Re, and Sc and highly negatively correlated with Kr and t. As earlier, we can observe that all parameters are significant.

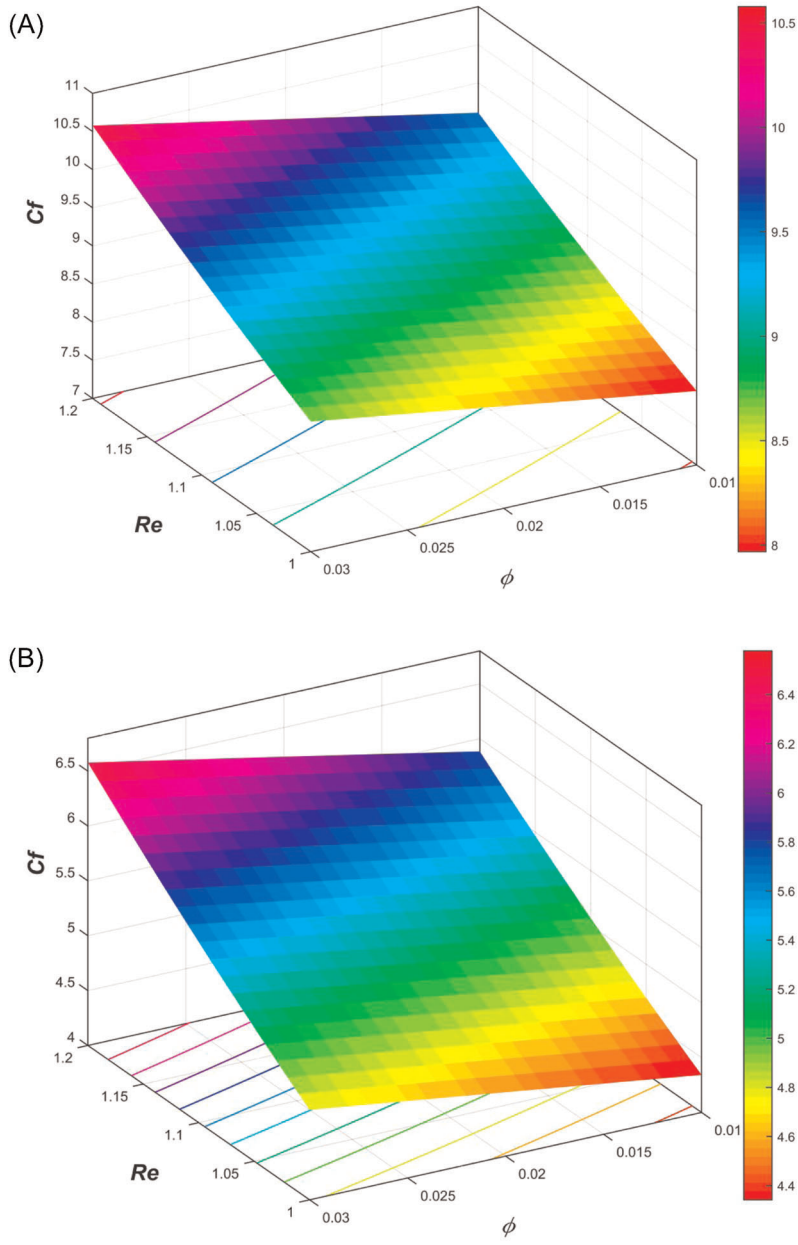

FIGURE 11 (A) Parallel effect of ϕ and Re on Cf for plate at $y = 0$. (B) Parallel effect of ϕ and Re on Cf for plate at $y = 1$ [Color figure can be viewed at wileyonlinelibrary.com]

6.2 | Regression analysis

All correlations are perceived to be significant and hence further analysis can be carried out using regression. Nu and Sh are estimated using multiple linear regression models. The estimated models are of the form:

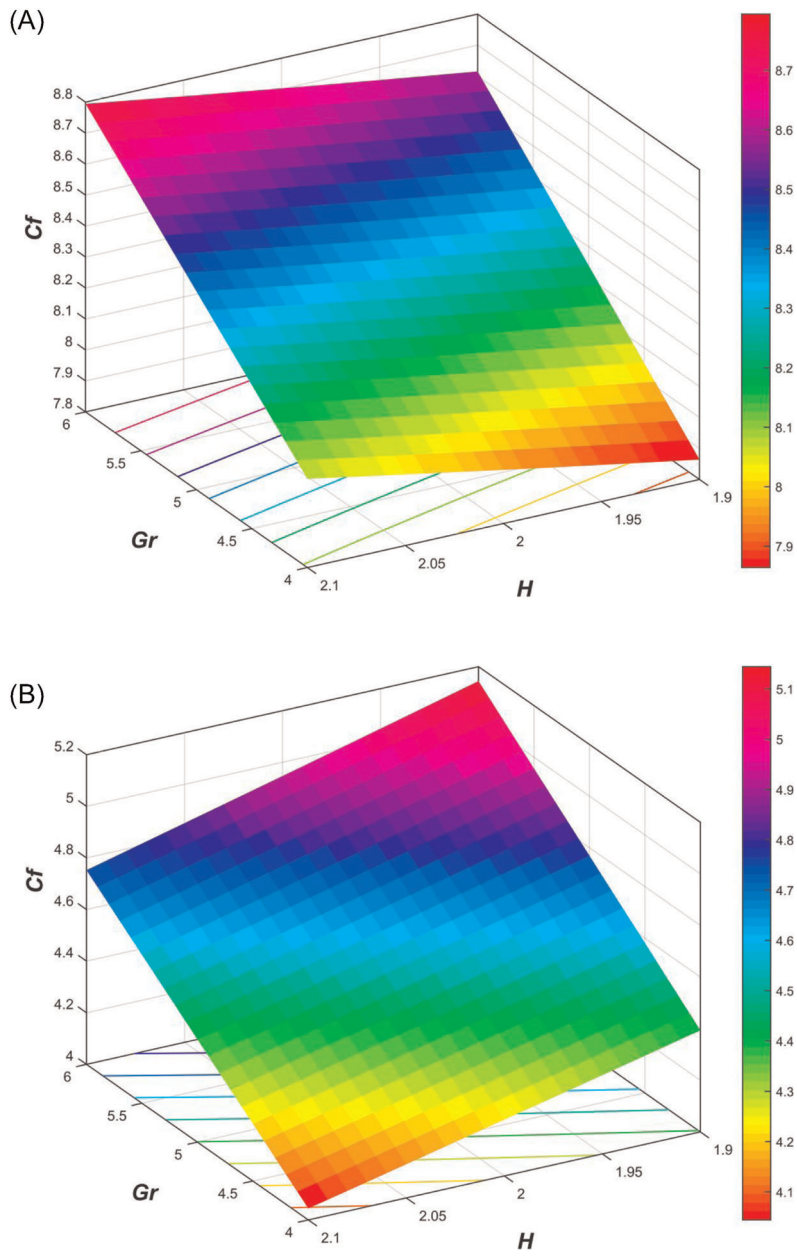

FIGURE 12 (A) Parallel effect of H and Gr on Cf for plate at $y = 0$. (B) Parallel effect of H and Gr on Cf for plate at $y = 1$ [Color figure can be viewed at wileyonlinelibrary.com]

$$Nu_{est} = b_t t + b_\phi \phi + b_\omega \omega + b_{Re} Re + c$$

$$Sh_{est} = b_t t + b_\omega \omega + b_{Re} Re + b_{Sc} Sc + b_{Kr} Kr + c$$

where c, b_t, b_ϕ, b_ω, b_{Re}, b_{Sc} and b_{Kr} are the estimated regression coefficients.

Nu and Sh is estimated from 30 sets of values chosen in the range [0,0.04] for ϕ, [5,15] for ω, [1,1.2] for Re, [0.2,1] for Sc, [0.5,2] for Kr, and [0.5, $\frac{\pi}{2}$] for t and the regression coefficients are

TABLE 5 Correlation coefficient (r), probable error (PE) and $|r/PE|$ values of Nu at $y = 1$ with respect to the parameters ϕ, ω, Re, and t

Parameter	r	PE	$\left\|\frac{r}{PE}\right\|$
ϕ	−0.998525054	0.000889166	1122.990857
ω	−0.96135646	0.025561445	37.60962927
Re	0.999999168	5.02117E−07	1991567.608
t	0.999450864	0.000427575	2337.487341

TABLE 6 Correlation coefficient (r), probable error (PE) and $|r/PE|$ values of Sh at $y = 1$ with respect to the parameters ω, Re, Sc, Kr, and t

Parameter	r	PE	$\left\|\frac{r}{PE}\right\|$
ω	0.999963802	2.44153E−05	40,956.47543
Re	0.999998301	1.02471E−06	975,880.9088
Sc	0.999968876	1.87766E−05	53,256.12316
Kr	−0.999947742	3.52471E−05	28,369.64913
t	−0.991117969	0.006887008	143.9112518

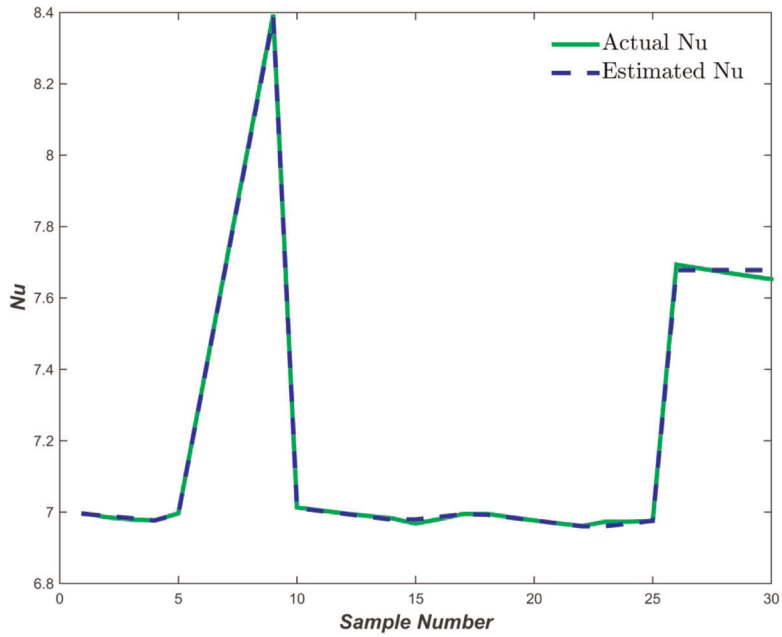

FIGURE 13 Actual Nu versus estimated Nu [Color figure can be viewed at wileyonlinelibrary.com]

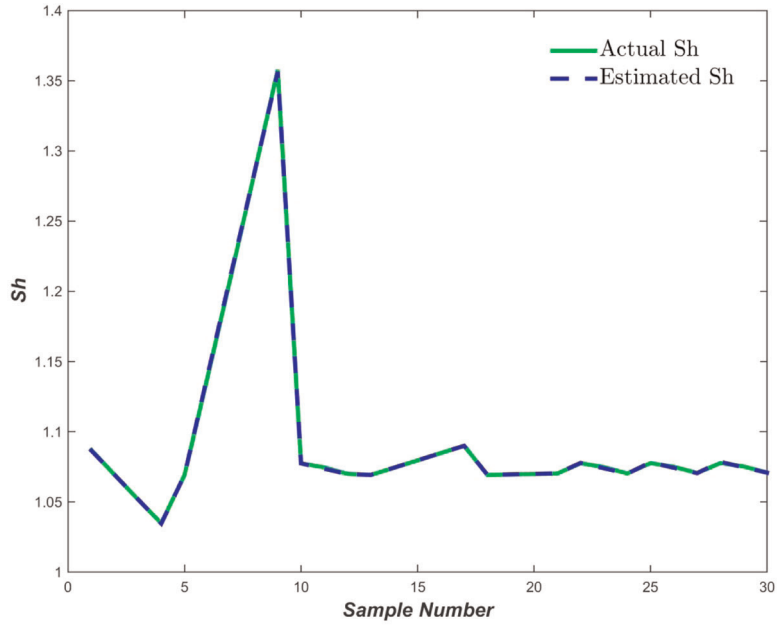

FIGURE 14 Actual *Sh* versus estimated *Sh* [Color figure can be viewed at wileyonlinelibrary.com]

found using Microsoft Excel. As the *p*-values for all the physical parameters are less than 0.05, the regression coefficients are significant. The estimated regression models are given by:

$$Nu_1^{est} = 0.014996t - 0.807981\phi - 0.006215\omega + 6.953733Re + 0.065176$$

$$Sh_1^{est} = -0.007645t + 0.000344\omega + 0.103518Re + 0.359017Sc - 0.034689Kr + 0.938922$$

A negative sign of the estimated regression coefficient implies that the corresponding parameter reduces the corresponding physical quantity. The estimated regression equation corresponds to the results achieved in Tables 3 and 4. Figures 13 and 14 illustrate the accuracy of the regression model for the chosen sample.

7 | CONCLUSION

The main conclusions drawn from the current study are listed below:

- The main flow velocity profile is directly proportional to Grashof number (Gr), the volume fraction of nanoparticle (ϕ), and modified Grashof number (Gm).
- The main flow velocity profile is greater when the magnetic field is applied on the upward moving plate as compared to the main flow velocity when the magnetic field is applied on the downward-moving plate.
- The injection parameter (Re) has a constructive effect on the main flow velocity.
- The injection parameter enhances the temperature profile, whereas the nanoparticle volume fraction diminishes the temperature profile.

- On the upward moving plate, the main flow velocity profile exhibits a mixed behavior when Hartmann number (H) is increased. Initially, the velocity reduces and after traveling a certain length the velocity increases.
- On the downward-moving plate, the velocity profile is inversely proportional to the Hartmann number·
- Schmidt number has a constructive effect on the concentration profile.
- Nusselt number is highly positively correlated with the injection parameter and highly negatively correlated with nanoparticle volume fraction.
- The regression models are found to be faultless for the chosen range of values of the parameters.

NOMENCLATURE

B_0	strength of the magnetic field
C^*	fluid concentration (Moles/kg)
$\mathcal{C}_0$	nanoparticle concentration near the plate at origin (Moles/kg)
$\mathcal{C}_1$	nanoparticle concentration near the plate at d (Moles/kg)
C_p	specific heat at constant pressure
d	distance between the plates
D_B	chemical molecular diffusivity (m^2/s)
g	acceleration due to gravity (m/s^2)
K_l	chemical reaction parameter
p^*	pressure
t^*	time (s)
T^*	fluid temperature (K)
T_0	temperature of the fluid near the plate at origin (K)
T_1	temperature of the fluid near the plate at d (K)
u^*, v^*, w^*	velocity components (m/s)
U_0	velocity of the moving plates
V_0	injection velocity

GREEK SYMBOLS

σ	electrical conductivity
ϕ	volume fraction of nanoparticles
μ	dynamic viscosity (kg/m s)
ρ	density (kg/m^3)
ϑ	kinematic viscosity (m^2/s)
ω^*	angular velocity
κ	thermal conductivity (W/m K)
$\varepsilon_0, \varepsilon_1, \varepsilon_2$	very small reference constants

NONDIMENSIONAL QUANTITIES

Gm $\frac{g\beta_f \vartheta_f (\mathcal{C}_0 - \mathcal{C}_1)}{U_0 V_0^2}$; Modified Grashof number

Gr $\frac{g\beta_f \vartheta_f (T_0 - T_1)}{U_0 V_0^2}$; Grashof number

H $B_0 d\sqrt{\frac{\sigma_f}{\rho_f \vartheta_f}}$; Hartmann number

Kr $\frac{K_l d^2}{\vartheta_f}$; chemical reaction parameter

Pr $\frac{(\mu c_p)_f}{\kappa_f}$; Prandtl number

Re $\frac{V_0 d}{\vartheta_f}$; injection/suction parameter

Sc $\frac{\vartheta_f}{D_B}$; Schmidt number

SUBSCRIPTS

f base fluid
nf nanofluid
s nanoparticle

ACKNOWLEDGMENT

The authors acknowledge learned reviewers for their thoughtful comments and constructive suggestions.

ORCID

Sujesh Areekara http://orcid.org/0000-0001-7860-8268
Alphonsa Mathew http://orcid.org/0000-0002-3810-4484

REFERENCES

1. Sabu AS, Mathew A, Neethu TS, Anil George K. Statistical analysis of MHD convective ferro-nanofluid flow through an inclined channel with hall current, heat source and soret effect. *Therm Sci Eng Prog*. 2021;22:100816. https://doi.org/10.1016/j.tsep.2020.100816
2. Kumar MA, Reddy YD, Rao VS, Goud BS. Thermal radiation impact on MHD heat transfer natural convective nano fluid flow over an impulsively started vertical plate. *Case Stud Therm Eng*. 2021;24:100826. https://doi.org/10.1016/j.csite.2020.100826
3. Jha BK, Aina B. Magnetohydrodynamic natural convection flow in a vertical micro-porous-channel in the presence of induced magnetic field. *Commun Nonlinear Sci Numer Simul*. 2018;64:14-34. https://doi.org/10.1016/j.cnsns.2018.04.004
4. Jha BK, Aina B. Role of induced magnetic field on MHD natural convection flow in vertical microchannel formed by two electrically non-conducting infinite vertical parallel plates. *Alexandria Eng J*. 2016;55:2087-2097. https://doi.org/10.1016/j.aej.2016.06.030
5. Jha BK, Isah BY, Uwanta IJ. Combined effect of suction/injection on MHD free-convection flow in a vertical channel with thermal radiation. *Ain Shams Eng J*. 2018;9:1069-1088. https://doi.org/10.1016/j.asej.2016.06.001
6. Jha BK, Aina B. Impact of induced magnetic field on magnetohydrodynamic (MHD) natural convection flow in a vertical annular micro-channel in the presence of radial magnetic field. *Propuls Power Res*. 2018;7:171-181. https://doi.org/10.1016/j.jppr.2018.04.004
7. Das S, Jana RN, Makinde OD. Transient natural convection in a vertical channel filled with nanofluids in the presence of thermal radiation. *Alexandria Eng J*. 2016;55:253-262. https://doi.org/10.1016/j.aej.2015.10.013
8. Jha BK, Malgwi PB, Aina B. Hall effects on MHD natural convection flow in a vertical microchannel. *Alexandria Eng J*. 2018;57:983-993. https://doi.org/10.1016/j.aej.2017.01.038

9. Zainal NA, Nazar R, Naganthran K, Pop I. Stability analysis of MHD hybrid nanofluid flow over a stretching/shrinking sheet with quadratic velocity. *Alexandria Eng J*. 2021;60:915-926. https://doi.org/10.1016/j.aej.2020.10.020
10. Elayarani M, Shanmugapriya M, Senthil Kumar P. Intensification of heat and mass transfer process in MHD carreau nanofluid flow containing gyrotactic microorganisms. *Chem Eng Process—Process Intensif*. 2021;160:108299. https://doi.org/10.1016/j.cep.2021.108299
11. Biswal U, Chakraverty S, Ojha BK, Hussein AK. Numerical simulation of magnetohydrodynamics nanofluid flow in a semi-porous channel with a new approach in the least square method. *Int Commun Heat Mass Transf*. 2021;121:105085. https://doi.org/10.1016/j.icheatmasstransfer.2020.105085
12. Raju T Linga. MHD heat transfer two-ionized fluids flow between parallel plates with Hall currents. *Results Eng*. 2019;4:100043. https://doi.org/10.1016/j.rineng.2019.100043
13. Ahmed S, Zueco J, López-González LM. Numerical and analytical solutions for magneto-hydrodynamic 3D flow through two parallel porous plates. *Int J Heat Mass Transf*. 2017;108:322-331. https://doi.org/10.1016/j.ijheatmasstransfer.2016.11.102
14. Dash GC, Ojha KL. Viscoelastic hydromagnetic flow between two porous parallel plates in the presence of sinusoidal pressure gradient. *Alexandria Eng J*. 2018;57:3463-3471. https://doi.org/10.1016/j.aej.2017.12.011
15. Venkatesh LP. Suction Injection Induced MHD fow through vertical narrow porous channel with permeable properties. *Int J Recent Technol Eng*. 2019;8:121-126. https://doi.org/10.35940/ijrte.c6404.118419
16. Singh KD, Sharma R. Three-dimensional flow between two parallel porous plates with heat transfer. *Zeitschrift Fur Naturforsch—Sect A J Phys Sci*. 2001;56:596-600. https://doi.org/10.1515/zna-2001-0809
17. Attia HA, Kotb NA. MHD flow between two parallel plates with heat transfer. *Acta Mech*. 1996;117:215-220. https://doi.org/10.1007/BF01181049
18. López A, Ibáñez G, Pantoja J, Moreira J, Lastres O. Entropy generation analysis of MHD nanofluid flow in a porous vertical microchannel with nonlinear thermal radiation, slip flow and convective-radiative boundary conditions. *Int J Heat Mass Transf*. 2017;107:982-994. https://doi.org/10.1016/j.ijheatmasstransfer.2016.10.126
19. Dogonchi AS, Divsalar K, Ganji DD. Flow and heat transfer of MHD nanofluid between parallel plates in the presence of thermal radiation. *Comput Methods Appl Mech Eng*. 2016;310:58-76. https://doi.org/10.1016/j.cma.2016.07.003
20. Hassan AR. The entropy generation analysis of a reactive hydromagnetic couple stress fluid flow through a saturated porous channel. *Appl Math Comput*. 2020;369:124843. https://doi.org/10.1016/j.amc.2019.124843
21. Bhattacharyya A, Kumar R, Seth GS. Capturing the features of peristaltic transport of a chemically reacting couple stress fluid through an inclined asymmetric channel with Dufour and Soret effects in presence of inclined magnetic field. *Indian J Phys*. 2021. https://doi.org/10.1007/s12648-020-01936-8
22. Kiyani MZ, Hayat T, Ahmad I, Waqas M, Alsaedi A. Bidirectional Williamson nanofluid flow towards stretchable surface with modified Darcy's law. *Surface Interfaces*. 2021;23:100872. https://doi.org/10.1016/j.surfin.2020.100872
23. Kumar R, Bhattacharyya A, Seth GS, Chamkha AJ. Transportation of magnetite nanofluid flow and heat transfer over a rotating porous disk with Arrhenius activation energy: fourth order Noumerov's method. *Chinese J Phys*. 2021;69:172-185. https://doi.org/10.1016/j.cjph.2020.11.018
24. Hazarika S, Ahmed S, Chamkha AJ. Investigation of nanoparticles Cu, Ag and Fe_3O_4 on thermophoresis and viscous dissipation of MHD nanofluid over a stretching sheet in a porous regime: a numerical modeling. *Math Comput Simul*. 2021;182:819-837. https://doi.org/10.1016/j.matcom.2020.12.005
25. Seth GS, Bhattacharyya A, Kumar R, Chamkha AJ. Entropy generation in hydromagnetic nanofluid flow over a non-linear stretching sheet with Navier's velocity slip and convective heat transfer. *Phys Fluids*. 2018;30:122003. https://doi.org/10.1063/1.5054099
26. Mackolil J, Mahanthesh B. Exact and statistical computations of radiated flow of nano and Casson fluids under heat and mass flux conditions. *J Comput Des Eng*. 2019;6:593-605. https://doi.org/10.1016/j.jcde.2019.03.003
27. Hayat T, Khan MI, Qayyum S, Alsaedi A. Modern developments about statistical declaration and probable error for skin friction and Nusselt number with copper and silver nanoparticles. *Chinese J Phys*. 2017;55:2501-2513. https://doi.org/10.1016/j.cjph.2017.08.028

28. Mackolil J, Mahanthesh B. Sensitivity analysis of radiative heat transfer in Casson and nano fluids under diffusion-thermo and heat absorption effects. *Eur Phys J Plus*. 2019;134:619. https://doi.org/10.1140/epjp/i2019-12949-6
29. Jahan S, Sakidin H, Nazar R, Pop I. Analysis of heat transfer in nanofluid past a convectively heated permeable stretching/shrinking sheet with regression and stability analyses. *Results Phys*. 2018;10:395-405. https://doi.org/10.1016/j.rinp.2018.06.021
30. Mahanthesh B, Shashikumar NS, Gireesha BJ, Animasaun IL. Effectiveness of Hall current and exponential heat source on unsteady heat transport of dusty TiO_2-EO nanoliquid with nonlinear radiative heat. *J Comput Des Eng*. 2019;6:551-561. https://doi.org/10.1016/j.jcde.2019.04.005
31. Mahanthesh B, Mackolil J, Shehzad SA. Statistical analysis of stagnation-point heat flow in Williamson fluid with viscous dissipation and exponential heat source effects. *Heat Transf*. 2020;49:4580-4591. https://doi.org/10.1002/htj.21842
32. Sabu AS, Areekara S, Mathew A. Statistical analysis on three-dimensional MHD convective Carreau nanofluid flow due to bilateral nonlinear stretching sheet with heat source and zero mass flux condition. *Heat Transf*. 2020. https://doi.org/10.1002/htj.22045
33. Singh K, Mathew A. Three dimensional MHD fluctuating free convective flow between two vertical porous plates moving in opposite directions. *J Rajasthan Acad Phys Sci*. 2009;8:457-474.
34. Gupta VG, Jain A, Jha AK. Convective effects on MHD flow and heat transfer between vertical plates moving in opposite direction and partially filled with a porous medium. *J Appl Math Phys*. 2016;4:341-358. https://doi.org/10.4236/jamp.2016.42041
35. Gupta U, Jha AK, Chaudhary RC. Free convection flow between vertical plates moving in opposite direction and partially filled with porous medium. *Appl Math*. 2011;2:935-941. https://doi.org/10.4236/am.2011.28128
36. Singh K, Mathew A. Heat transfer in three dimensional MHD flow between two parallel porous plates moving in opposite directions with transpiration cooling. *Proc Natl Acad Sci India Sect A—Phys Sci*. 2009;79:291-302.
37. Fisher R. On the "Probable Error" of a coefficient of correlation deduced from a small sample. *Metron*. 1921;1:1-32. https://ci.nii.ac.jp/naid/10012392243/en/

How to cite this article: Neethu TS, Areekara S, Mathew A. Statistical approach on 3D hydromagnetic flow of water-based nanofluid between two vertical porous plates moving in opposite directions. *Heat Transfer*. 2021;1-28. https://doi.org/10.1002/htj.22120

APPENDIX

$$a = \frac{A_5 PrRe}{A_6}$$

$$m_1 = \frac{ScRe + \sqrt{Sc^2Re^2 + 4ScKr}}{2}$$

$$m_2 = \frac{ScRe - \sqrt{Sc^2Re^2 + 4ScKr}}{2}$$

$$m_3 = \frac{A_1A_2Re + \sqrt{A_1^2A_2^2Re^2 + 4A_1A_3H^2}}{2}$$

$$m_4 = \frac{A_1A_2Re - \sqrt{A_1^2A_2^2Re^2 + 4A_1A_3H^2}}{2}$$

$$r_1 = \frac{m_3 + \sqrt{m_3^2 + 4\pi^2}}{2}$$

$$r_2 = \frac{m_3 - \sqrt{m_3^2 + 4\pi^2}}{2}$$

$$r_3 = \frac{m_4 + \sqrt{m_4^2 + 4\pi^2}}{2}$$

$$r_4 = \frac{m_4 - \sqrt{m_4^2 + 4\pi^2}}{2}$$

$$B_1 = \frac{A_1A_2A_4Re^2\,Gr}{(e^a - 1)(a^2 - A_1A_2Rea - A_1A_3H^2)}$$

$$B_2 = \frac{A_1A_2A_4Re^2\,Gme^{m_2}}{\left(e^{m_1} - e^{m_2}\right)\left(m_1^2 - A_1A_2Rem_1 - A_1A_3H^2\right)}$$

$$B_3 = \frac{A_1A_2A_4Re^2\,Gme^{m_1}}{\left(e^{m_2} - e^{m_1}\right)\left(m_2^2 - A_1A_2Rem_2 - A_1A_3H^2\right)}$$

$$B_4 = \frac{A_1A_2A_4Re^2\,Gre^a}{(e^a - 1)A_1A_3H^2)}$$

$$\alpha_1 = -(B_1 + B_2 + B_3 + B_4)$$

$$\beta_1 = -2 - (B_1e^a + B_2e^{m_1} + B_3e^{m_2} + B_4)$$

$$r_5 = \frac{A_1A_2Re + \sqrt{A_1^2A_2^2Re^2 + 4(i\omega A_1A_2 + A_1A_3H^2)}}{2}$$

$$r_6 = \frac{A_1A_2Re - \sqrt{A_1^2A_2^2Re^2 + 4(i\omega A_1A_2 + A_1A_3H^2)}}{2}$$

$$D = D_1 + D_2 + D_3 + D_4$$

$$D_1 = r_3r_4(e^{r_2+r_4} - e^{r_2+r_3}) + r_2r_4(e^{r_3+r_2} - e^{r_3+r_4}) + r_2r_3(e^{r_3+r_4} - e^{r_2+r_4})$$

$$D_2 = r_3r_4(e^{r_1+r_3} - e^{r_1+r_4}) + r_1r_4(e^{r_3+r_4} - e^{r_3+r_1}) + r_1r_3(e^{r_1+r_4} - e^{r_3+r_4})$$

$$D_3 = r_2r_4(e^{r_1+r_4} - e^{r_1+r_2}) + r_1r_4(e^{r_2+r_1} - e^{r_2+r_4}) + r_1r_2(e^{r_2+r_4} - e^{r_1+r_4})$$

$$D_4 = r_2r_3(e^{r_1+r_2} - e^{r_1+r_3}) + r_1r_3(e^{r_3+r_2} - e^{r_2+r_1}) + r_1r_2(e^{r_1+r_3} - e^{r_2+r_3})$$

$$m_5 = \frac{ScRe + \sqrt{Sc^2Re^2 + 4Sc(i\omega + Kr)}}{2}$$

$$m_6 = \frac{ScRe - \sqrt{Sc^2Re^2 + 4Sc(i\omega + Kr)}}{2}$$

$$n_1 = \frac{\left(\frac{A_5PrRe}{A_6} + \sqrt{\frac{A_5^2Pr^2Re^2}{A_6^2} + \frac{4A_5Pr\omega i}{A_6}}\right)}{2}$$

$$n_2 = \frac{\left(\frac{A_5PrRe}{A_6} - \sqrt{\frac{A_5^2Pr^2Re^2}{A_6^2} + \frac{4A_5Pr\omega i}{A_6}}\right)}{2}$$

$$K_1 = \frac{A_1A_2A_4Re^2\,Gre^{n_2}}{(e^{n_1} - e^{n_2})\left(n_1^2 - A_1A_2Ren_1 - A_1A_2i\omega - A_1A_3H^2\right)}$$

$$K_2 = \frac{A_1A_2A_4Re^2\,Gre^{n_1}}{(e^{n_2} - e^{n_1})\left(n_2^2 - A_1A_2Ren_2 - A_1A_2i\omega - A_1A_3H^2\right)}$$

$$K_3 = \frac{A_1A_2A_4Re^2\,Gme^{m_6}}{(e^{m_5} - e^{m_6})\left(m_5^2 - A_1A_2Rem_5 - A_1A_2i\omega - A_1A_3H^2\right)}$$

$$K_4 = \frac{A_1A_2A_4Re^2\,Gme^{m_5}}{(e^{m_6} - e^{m_5})\left(m_6^2 - A_1A_2Rem_6 - A_1A_2i\omega - A_1A_3H^2\right)}$$

$$\alpha_2 = -(K_1 + K_2 + K_3 + K_4)$$

$$\beta_2 = -(K_1e^{n_1} + K_2e^{n_2} + K_3e^{m_5} + K_4e^{m_6})$$

$$n_3 = \frac{A_1A_2Re + \sqrt{A_1^2A_2^2Re^2 + 4(A_1A_3H^2 + \pi^2)}}{2}$$

$$n_4 = \frac{A_1A_2Re - \sqrt{A_1^2A_2^2Re^2 + 4(A_1A_3H^2 + \pi^2)}}{2}$$

$$K_{i1} = \frac{m_3(\alpha_1e^{m_4} - \beta_1)A_1A_2ReD_i}{(e^{m_4} - e^{m_3})D\left[(r_i + m_3)^2 - A_1A_2Re(r_i + m_3) - (A_1A_3H^2 + \pi^2)\right]},\ i = 1,2,3,4$$

$$K_{i2} = \frac{m_4(\beta_1 - \alpha_1e^{m_3})A_1A_2ReD_i}{(e^{m_4} - e^{m_3})D\left[(r_i + m_4)^2 - A_1A_2Re(r_i + m_4) - (A_1A_3H^2 + \pi^2)\right]},\ i = 1,2,3,4$$

$$M_{i1} = \frac{m_3((\alpha_1 + 2)e^{m_4} - (\beta_1 + 2))A_1A_2ReD_i}{(e^{m_4} - e^{m_3})D\left[(r_i + m_3)^2 - A_1A_2Re(r_i + m_3) - (A_1A_3H^2 + \pi^2)\right]},\ i = 1,2,3,4$$

$$M_{i2} = \frac{m_4((\beta_1 + 2) - (\alpha_1 + 2)e^{m_3})A_1A_2ReD_i}{(e^{m_4} - e^{m_3})D\left[(r_i + m_4)^2 - A_1A_2Re(r_i + m_4) - (A_1A_3H^2 + \pi^2)\right]},\ i = 1,2,3,4$$

$$M_{i3} = K_{i3} = \frac{aB_1A_1A_2ReD_i}{D\left[(r_i + a)^2 - A_1A_2Re(r_i + a) - (A_1A_3H^2 + \pi^2)\right]},\ i = 1,2,3,4$$

$$M_{i4} = K_{i4} = \frac{m_1 B_2 A_1 A_2 Re D_i}{D\left[(r_i + m_1)^2 - A_1 A_2 Re(r_i + m_1) - (A_1 A_3 H^2 + \pi^2)\right]}, i = 1,2,3,4$$

$$M_{i5} = K_{i5} = \frac{m_2 B_3 A_1 A_2 Re D_i}{D\left[(r_i + m_2)^2 - A_1 A_2 Re(r_i + m_2) - (A_1 A_3 H^2 + \pi^2)\right]}, i = 1,2,3,4$$

$$\alpha_3 = -\sum_{i=1}^{4}(K_{i1} + K_{i2} + K_{i3} + K_{i4} + K_{i5})$$

$$\beta_3 = -\sum_{i=1}^{4}(K_{i1}e^{r_i+m_3} + K_{i2}e^{r_i+m_4} + K_{i3}e^{r_i+a} + K_{i4}e^{r_i+m_1} + K_{i5}e^{r_i+m_2})$$

$$\alpha_4 = -\sum_{i=1}^{4}(M_{i1} + M_{i2} + M_{i3} + M_{i4} + M_{i5})$$

$$\beta_4 = -\sum_{i=1}^{4}(M_{i1}e^{r_i+m_3} + M_{i2}e^{r_i+m_4} + M_{i3}e^{r_i+a} + M_{i4}e^{r_i+m_1} + M_{i5}e^{r_i+m_2})$$